Subsurface nanodomains with in-plane polarization in uniaxial ferroelectrics via scanning force microscopy

N. A. Pertsev[1,*] and A. L. Kholkin[2,†]

[1]*A. F. Ioffe Physical-Technical Institute of the Russian Academy of Sciences and St. Petersburg State Polytechnical University, St. Petersburg, Russia*

[2]*Center for Research in Ceramics and Composite Materials (CICECO) and Department of Materials and Ceramic Engineering, University of Aveiro, Aveiro, Portugal*

(Received 25 June 2013; revised manuscript received 14 October 2013; published 21 November 2013)

Ferroelectric nanodomains can be created by the application of a bias voltage to the sharp conducting tip of a scanning force microscope (SFM) contacting the sample surface. Since an inhomogeneous electric field created by an SFM tip has maximum intensity along the surface normal, in multiaxial ferroelectrics the polarization inside these domains also tends to orient perpendicularly to the surface. Here we show theoretically that unusual domains can be created in uniaxial ferroelectrics when the SFM tip is applied to the crystal surface parallel to the polar axis. These 180° nanodomains have polarization directed along the surface and should appear in $LiNbO_3$ and $LiTaO_3$ crystals at moderate tip voltages well below 100 V. Calculations of equilibrium domain dimensions demonstrate that subsurface domains have the shape of a needle oriented along the polar axis.

DOI: 10.1103/PhysRevB.88.174109 PACS number(s): 77.80.Dj, 77.80.Fm

I. INTRODUCTION

Ferroelectric domains are distinguished by very thin boundaries (domain walls), typically having a width of the order of one to two lattice constants only.[1,2] This feature allows the creation of nanoscale domains and opens the way for the development of nonvolatile memories with ultrahigh (>10 Tbit/in^2) storage densities.[3,4] The writing of ferroelectric nanodomains can be performed using a scanning force microscope (SFM) in the contact mode and applying sufficient direct current voltage between the sharp conducting tip and bottom electrode.[5,6] The same setup allows the imaging of written domains, which requires the application of small alternating current voltage to the SFM tip, and the measurement of surface displacements caused by the converse piezoelectric effect (piezoresponse force microscopy).[6]

The tip-induced formation of ferroelectric domains in bulk crystals and thin films is well understood.[7–11] However, the theoretical studies have been mostly devoted to 180° domains with the polarization orthogonal to the sample surface because this situation corresponds to the maximum intensity of electric field created by the SFM tip. Owing to this feature, the tip-induced field is expected to promote a non-180° switching in multiaxial ferroelectrics when the initial polarization is parallel to the surface. In uniaxial ferroelectrics such as $LiNbO_3$ and $LiTaO_3$, however, only the 180° polarization reversal is allowed so that the domain writing becomes questionable when the tip is applied to the crystal surface parallel to the polar axis. It should be emphasized that $LiNbO_3$ and $LiTaO_3$ represent important ferroelectric materials, having applications in optoelectronics, diffractive and nonlinear optics,[12] frequency conversion devices,[13] and surface acoustic wave devices.[14]

In this paper, we analyze theoretically the possibility of creating domains by the application of a voltage to the SFM tip contacting the surface parallel to the polar axis of a uniaxial ferroelectric. To that end, an analytical expression is derived for the total energy of a subsurface 180° domain. The minimization of this energy with respect to the domain dimensions makes it possible to calculate the critical voltage necessary for the domain formation and to determine the evolution of equilibrium domain sizes under the voltages above the critical one. The numerical calculations performed for stoichiometric $LiNbO_3$ and $LiTaO_3$ crystals demonstrate that subsurface 180° domains should form at moderate tip voltages and have the shape of needles oriented in the polarization direction.

II. THEORETICAL CALCULATIONS

Consider a homogeneously polarized ferroelectric crystal subjected to an electric field $\mathbf{E}_{tip}$ of a biased SFM tip applied to the surface parallel to the polar axis. Since the field-induced switching in uniaxial ferroelectrics is limited to 180° reversal of the spontaneous polarization $\mathbf{P}_s$, the field $\mathbf{E}_{tip}$ may create only a 180° domain with the polarization parallel to the crystal surface (see Fig. 1). To calculate the energy of such a domain, we introduce the rectangular coordinate system (x, y, z) with the z axis perpendicular to the surface and the x axis parallel to the polar crystallographic direction. Taking into account that 180° domain walls in $LiTaO_3$ and $LiNbO_3$ are atomically thin,[15] we can write a change in the crystal free energy F after the polarization switching inside the domain volume Ω as

$$\Delta F = U_{dw} + U_{dep} - 2P_s \int_{\Omega} E_x^{tip}(x,y,z)d\Omega, \qquad (1)$$

where U_{dw} in the self-energy of the domain boundary, U_{dep} is the energy of a depolarizing field created by the polarization charges $\rho = -\mathrm{div}\mathbf{P}$ distributed along a curved domain boundary, and the last term represents the work W_{tip} done by $\mathbf{E}_{tip}$ during the polarization reversal inside Ω. It should be noted that the tip can be modeled by a circular cone with the height $H \sim 10\ \mu$m ending by a spherical apex having the radius of curvature $r_{tip} \sim$ 10–50 nm.[16]

To find ΔF via Eq. (1), one has to calculate the electric field created by the SFM tip inside the crystal ($z \leqslant 0$). In these electrostatic calculations, the ferroelectric crystal may

be modeled by a linear homogeneous anisotropic dielectric half-space $z \leqslant 0$ with the diagonal permittivity tensor ε_{ij} ($\varepsilon_{ii} = \varepsilon_i, \varepsilon_{ij} = 0$ at $i \neq j$), while the external medium (e.g., air or water) is assumed to have isotropic dielectric properties (relative permittivity ε_{ext}). Then the sought electric field can be computed by introducing an appropriate spatial distribution of point changes in the external medium $z > 0$.[16] The electrostatic potential $\phi(x, y, z)$ created by this charge distribution must have a constant value V on a surface modeling the tip shape and satisfy the continuity conditions on the interface plane $z = 0$. When the crystal surface is orthogonal to the symmetry axis providing transverse isotropy of the dielectric properties ($\varepsilon_x = \varepsilon_y$), the potential ϕ_{point} of a point charge needed for the calculation of $\mathbf{E}_{\text{tip}}$ acquires a simple form.[17] However, in our situation, the surface is parallel to the polar axis so that the dielectric response in the planes orthogonal to the surface normal is obviously anisotropic ($\varepsilon_x \neq \varepsilon_y$). In this case the exact solution for the point-charge potential becomes rather complicated even in the external isotropic medium.[18] Therefore, we will employ an approximate expression for $\phi_{\text{point}}(x, y, z)$ that makes it possible to develop an analytical description of the domain energetics.

The available theoretical results[17,19] suggest the following approximation for the potential induced *inside* an anisotropic half-space $z \leqslant 0$ by the charge q located at point ($x = y = 0$, $z = h$):

$$\phi_{\text{point}} \approx \frac{q}{2\pi\varepsilon_0(\varepsilon_{\text{ext}} + \sqrt{\varepsilon_x\varepsilon_z})\sqrt{x^2 + (\varepsilon_x/\varepsilon_y)y^2 + (h - \sqrt{\varepsilon_x/\varepsilon_z}z)^2}}, \tag{2}$$

where ε_0 is the permittivity of the vacuum. At $\varepsilon_x = \varepsilon_y$, this formula reduces to the exact solution for the potential of a point charge situated at a distance h above a semi-infinite transversely isotropic medium.[17] In addition, Eq. (2) allows for the influence of dielectric anisotropy on a solution to the Poisson's equation in an infinite medium, which involves the scaling $x' = x/\sqrt{\varepsilon_x}$, $y' = y/\sqrt{\varepsilon_y}$, and $z' = z/\sqrt{\varepsilon_z}$ of spatial coordinates.[17,19] Assuming that the potential distribution in the external isotropic medium $z \geqslant 0$ is not affected by additional crystal anisotropy $\varepsilon_x \neq \varepsilon_y$, we find that the continuity conditions for potential ϕ_{point} and electric displacement D_z on the interface plane $z = 0$ are satisfied along the line $y = 0$. Moreover, in the region $|y| \ll (\varepsilon_y/\varepsilon_x)\sqrt{x^2 + h^2}$ the steplike changes of ϕ_{point} and D_z occurring on $z = 0$ are much smaller than their values here. Therefore, the proposed solution is expected to have reasonable accuracy for the analysis of strongly elongated domains considered in this paper, provided we orient the x axis along the polarization direction.

The widely used model of SFM tip in the form of a *single point charge*,[7,8,11] however, is not suitable for the theoretical description of in-plane needle domains, because at distances $x \gg r_{\text{tip}}$ the main contribution to $\mathbf{E}_{\text{tip}}$ is created by the conical part of the tip. Therefore, we employ *line charge* model of the tip,[20,21] which allows for the long-range component of $\mathbf{E}_{\text{tip}}$ and makes it possible to derive an analytical expression for the interaction energy W_{tip}. Using Eq. (2) and integrating along a charged segment extending from $z = h$ to $z = H \gg h$, we obtain the potential created by the SFM tip inside a ferroelectric crystal ($z \leqslant 0$) in the form

$$\phi_{\text{tip}} \approx \frac{\lambda}{2\pi\varepsilon_0(\varepsilon_{\text{ext}} + \sqrt{\varepsilon_x\varepsilon_z})} \ln\left[\frac{H - \sqrt{\varepsilon_x/\varepsilon_z}z + \sqrt{x^2 + (\varepsilon_x/\varepsilon_y)y^2 + (H - \sqrt{\varepsilon_x/\varepsilon_z}z)^2}}{h - \sqrt{\varepsilon_x/\varepsilon_z}z + \sqrt{x^2 + (\varepsilon_x/\varepsilon_y)y^2 + (h - \sqrt{\varepsilon_x/\varepsilon_z}z)^2}}\right], \tag{3}$$

where λ represents the charge density per unit length. In Eq. (3), H may be set equal to the total tip height, whereas the parameters λ and h should be calculated from the electrostatic conditions at the tip apex. By analogy with the modified point charge model,[11] we determine these parameters by equating the potential $\phi_{\text{tip}}(x = 0, y = 0, z = \delta)$ at the apex to the bias voltage V and the curvature of equipotential surface at this point to $1/r_{\text{tip}}$ (δ is the distance between the tip apex and the crystal surface). The calculation shows that the position h of the charged segment bottom end can be found as a root of the cubic equation $2\sqrt{\varepsilon_x\varepsilon_z}h^3 - \varepsilon_{\text{ext}}(r_{\text{tip}} - 2\delta)h^2 - 2\sqrt{\varepsilon_x\varepsilon_z}\delta(r_{\text{tip}} + \delta)h - \varepsilon_{\text{ext}}\delta^2(r_{\text{tip}} + 2\delta) = 0$, which gives $h = (\varepsilon_{\text{ext}}/2\sqrt{\varepsilon_x\varepsilon_z})r_{\text{tip}}$ when the SFM tip is brought into contact with the crystal surface ($\delta = 0$). Substituting the calculated value of h into Eq. (3), one can find the charge density $\lambda \sim V$, which at $\delta = 0$ is defined by a simple formula $\lambda = 2\pi\varepsilon_0(\varepsilon_{\text{ext}} + \sqrt{\varepsilon_x\varepsilon_z})V/\ln[2\sqrt{\varepsilon_x\varepsilon_z}H/(\varepsilon_{\text{ext}}r_{\text{tip}})]$. It should be noted that the modified point charge model reproduces the tip-induced electric field in the vicinity of a spherical tip with a good accuracy.[11]

The differentiation of Eq. (3) with respect to the coordinate x yields the electric field intensity $E_x^{\text{tip}} = -\partial\phi_{\text{tip}}/\partial x$ along the polar axis. The calculation shows that E_x^{tip} has opposite signs on the right ($x > 0$) and left ($x < 0$) sides of the SFM tip and goes to zero at $x = 0$. In a homogeneously polarized uniaxial ferroelectric, therefore, the tip-induced electric field promotes the polarization reversal on one side of the SFM tip only. Moreover, as demonstrated by Fig. 2(a), the intensity E_x^{tip} reaches maximum at some distance $x = x_{\max}(y, z)$ from the tip and decreases relatively slowly at $x > x_{\max}$, having

the asymptotic behavior $E_x^{\text{tip}} \sim 1/x$ at $x \to \infty$. In contrast, the field intensity falls off rapidly along the y and z axes (see Fig. 2), decreasing as $1/y^2$ and $1/z^2$ in the limit of large y and z, respectively. These features indicate that the 180° domain created by the biased tip will be strongly elongated along the polar axis and localized in the subsurface layer. It may also be assumed that one of the domain ends is located just beneath the SFM tip (i.e., at the origin of the reference frame shown in Fig. 1).

To simplify further calculations, we approximate the domain shape by a half of a triaxial ellipsoid exscinded by the crystal surface. This model enables us to evaluate the depolarizing field energy U_{dep} via modification of the formula derived by Landauer for a semiellipsoidal domain extending into the crystal from the ferroelectric-metal interface.[19] Using electrostatic considerations based on the method of image charges[22] and allowing for scaling caused by dielectric anisotropy, we find

$$U_{\text{dep}} \approx \frac{\pi P_s^2}{3\varepsilon_0\varepsilon_x} \frac{\left(\frac{\varepsilon_z}{\varepsilon_y}\right)^{3/2} L w^2 d^2}{\left(\frac{\varepsilon_z}{\varepsilon_x}L^2 - 2\sqrt{\frac{\varepsilon_z}{\varepsilon_y}}wd\right)^{3/2}} \left[\sqrt{\frac{\varepsilon_z}{\varepsilon_x}}L \ln\left(\frac{\sqrt{\frac{\varepsilon_z}{\varepsilon_x}}L + \sqrt{\frac{\varepsilon_z}{\varepsilon_x}L^2 - 2\sqrt{\frac{\varepsilon_z}{\varepsilon_y}}wd}}{\sqrt{\frac{\varepsilon_z}{\varepsilon_x}}L - \sqrt{\frac{\varepsilon_z}{\varepsilon_x}L^2 - 2\sqrt{\frac{\varepsilon_z}{\varepsilon_y}}wd}}\right) - 2\sqrt{\frac{\varepsilon_z}{\varepsilon_x}L^2 - 2\sqrt{\frac{\varepsilon_z}{\varepsilon_y}}wd}\right], \tag{4}$$

where L is the domain length along the polar axis, w is the domain width set equal to its maximal extension on the surface in the transverse direction, and d is the maximum domain size in the direction orthogonal to the surface (see Fig. 1). Since the surface area of a triaxial ellipsoid may be calculated from the well-known approximate analytical formula, the self-energy U_{dw} of the domain boundary can be written as

$$U_{\text{dw}} \approx 2\pi \left[\frac{1}{3}\left(\frac{Lw}{4}\right)^{\beta} + \frac{1}{3}\left(\frac{Ld}{2}\right)^{\beta} + \frac{1}{3}\left(\frac{wd}{2}\right)^{\beta}\right]^{1/\beta} \gamma, \tag{5}$$

where $\beta \cong 1.6075$ and γ denotes the mean specific energy of a curved 180° wall bounding the considered domain. Finally, the last term in Eq. (1) may be evaluated with the aid of the mean value theorem. The calculation gives $W_{\text{tip}} = 2P_s S[\phi_{\text{tip}}(x^{**}, y^*, z^*) - \phi_{\text{tip}}(x^*, y^*, z^*)]$, where $S = (\pi/4)wd$ is the area of the domain cross section by the plane $x = L/2$, y^* and z^* are the coordinates of a point on this plane situated inside domain, and $x^{**} = (L/2)(1 + \sqrt{1 - 4y^{*2}/w^2 - z^{*2}/d^2})$ and $x^* = (L/2)(1 - \sqrt{1 - 4y^{*2}/w^2 - z^{*2}/d^2})$ represent the coordinates x of two points at which the line ($y = y^*$, $z = z^*$) crosses the domain boundary. Setting in the first approximation $y^* \approx w/4$ and $z^* \approx -d/2$ and using Eq. (3), we obtain

$$W_{\text{tip}} \approx -V P_s \tilde{\lambda} \frac{\pi wd}{2} \left[\ln\left(\frac{2\sqrt{\frac{\varepsilon_x}{\varepsilon_z}}d + 4H + \sqrt{2(3-2\sqrt{2})L^2 + \frac{\varepsilon_x}{\varepsilon_y}w^2 + 4\left(\sqrt{\frac{\varepsilon_x}{\varepsilon_z}}d + 2H\right)^2}}{2\sqrt{\frac{\varepsilon_x}{\varepsilon_z}}d + 4h + \sqrt{2(3-2\sqrt{2})L^2 + \frac{\varepsilon_x}{\varepsilon_y}w^2 + 4\left(\sqrt{\frac{\varepsilon_x}{\varepsilon_z}}d + 2h\right)^2}}\right)\right.$$
$$\left. - \ln\left(\frac{2\sqrt{\frac{\varepsilon_x}{\varepsilon_z}}d + 4H + \sqrt{2(3+2\sqrt{2})L^2 + \frac{\varepsilon_x}{\varepsilon_y}w^2 + 4\left(\sqrt{\frac{\varepsilon_x}{\varepsilon_z}}d + 2H\right)^2}}{2\sqrt{\frac{\varepsilon_x}{\varepsilon_z}}d + 4h + \sqrt{2(3+2\sqrt{2})L^2 + \frac{\varepsilon_x}{\varepsilon_y}w^2 + 4\left(\sqrt{\frac{\varepsilon_x}{\varepsilon_z}}d + 2h\right)^2}}\right)\right], \tag{6}$$

where $\tilde{\lambda} = \lambda/[2\pi\varepsilon_0(\varepsilon_{\text{ext}} + \sqrt{\varepsilon_x\varepsilon_z})V]$ is the normalized charge density independent of the bias voltage V.

The substitution of Eqs. (4)–(6) into Eq. (1) yields an analytic expression for the domain energy ΔF. By minimizing the function $\Delta F(L, w, d)$ numerically, it is possible to evaluate the critical bias voltage V_{cr} at which the domain formation becomes energetically favorable and to calculate the equilibrium domain length L^*, width w^*, and "depth" d^* at voltages $V \geqslant V_{\text{cr}}$. It should be emphasized that the modeling of domain shape by half of a triaxial ellipsoid enables us to allow for both the highly anisotropic three-dimensional distribution of the electric field E_x induced by the SFM tip along the polar axis and the influence of the depolarizing field energy tending to elongate the formed domain in the polarization direction.

In conclusion of this section, we note that the relation between in-plane and out-of-plane components of the tip-induced electric field depends on the dielectric anisotropy of the probed material. For uniaxial ferroelectrics with weak or moderate anisotropy, which are considered in this paper, the differentiation of Eq. (3) shows that the maximum value of E_z is several times higher than that of E_x (almost three times in $LiTaO_3$ and about two times in $LiNbO_3$). However, very strong anisotropy of the form $\varepsilon_z/\varepsilon_x \gg 1$ reverses the situation, as happens in the case of a $BaTiO_3$ crystal with the polar axis parallel to the surface ($\varepsilon_z/\varepsilon_x > 30$), where the in-plane component E_x becomes stronger than E_z.[23]

III. RESULTS AND DISCUSSION

We performed numerical calculations for stoichiometric $LiNbO_3$ and $LiTaO_3$ crystals using the experimental values of spontaneous polarization and dielectric constants compiled

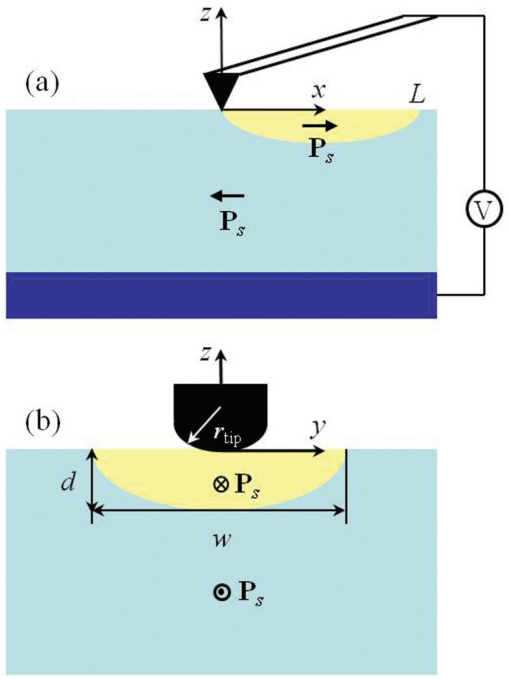

FIG. 1. (Color online) Schematic depiction of a subsurface 180° domain forming in a uniaxial ferroelectric subjected to an inhomogeneous electric field of a biased SFM tip applied to the surface parallel to the polar axis. (a) Overall view of the sample transverse section by the plane orthogonal to the crystal surface and parallel to the polarization direction (axis x). (b) Enlarged view of the domain cross section in the plane $x = L/2$.

in Ref. 24: $P_s \approx 0.75$ C/m^2, $\varepsilon_x \approx 29$, $\varepsilon_y = \varepsilon_z \approx 84$ for $LiNbO_3$, and $P_s \approx 0.55$ C/m^2, $\varepsilon_x \approx 44$, $\varepsilon_y = \varepsilon_z \approx 53$ for $LiTaO_3$. For the specific domain wall energy γ, we employed the values of 170 mJ/m^2 ($LiNbO_3$) and 60 mJ/m^2 ($LiTaO_3$) evaluated using the Landau-Ginzburg-Devonshire theory and the measured wall widths.[24] It should be noted that the result obtained for γ in $LiNbO_3$ was recently confirmed by simulations based on the density functional theory.[25]

The calculations covered the cases of sharp ($r_{tip} = 10$ nm) and blunt ($r_{tip} = 50$ nm) SFM tips in direct contact ($\delta = 0$, $H = 10$ μm) with surfaces of ferroelectric crystals immersed in air ($\varepsilon_{ext} = 1$) and water ($\varepsilon_{ext} = 81$). Table I summarizes the theoretical results obtained for the critical voltage V_{cr}. It can be seen that the moderate tip voltages well below 100 V appear to be sufficient for the formation of 180° domains with in-plane polarization in both $LiNbO_3$ and $LiTaO_3$. Remarkably, the tip radius r_{tip} does not affect the critical voltage significantly when the crystal is surrounded by air or vacuum. At the same time,

TABLE I. Calculated critical voltages for the formation of subsurface 180° domains with in-plane polarization in uniaxial ferroelectrics.

Conditions	V_{cr} for $LiNbO_3$ (V)	V_{cr} for $LiTaO_3$ (V)
$r_{tip} = 10$ nm, $\varepsilon_{ext} = 1$	19	12
$r_{tip} = 10$ nm, $\varepsilon_{ext} = 81$	39	25
$r_{tip} = 50$ nm, $\varepsilon_{ext} = 1$	21	13
$r_{tip} = 50$ nm, $\varepsilon_{ext} = 81$	58	37

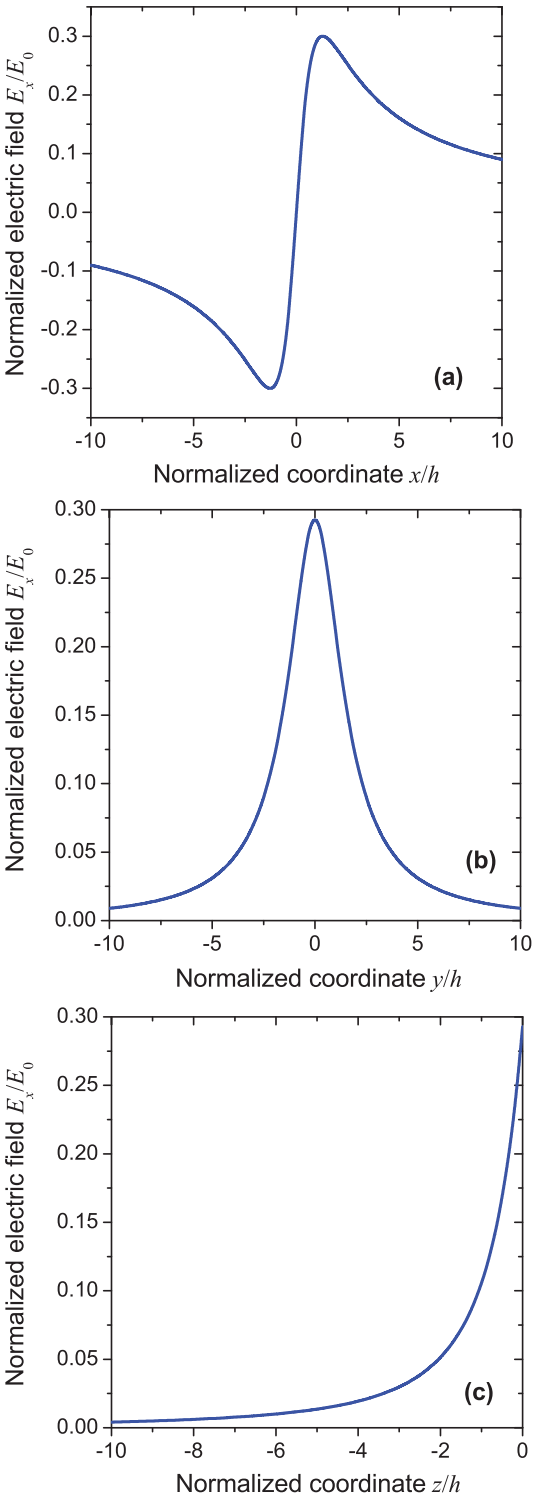

FIG. 2. (Color online) Electric field created by the SFM tip in the direction parallel to the surface. The field intensity E_x^{tip} is normalized by the quantity $E_0 = \lambda/[2\pi\varepsilon_0(\varepsilon_{ext} + \sqrt{\varepsilon_x\varepsilon_z})h]$. Panel (a) shows E_x^{tip} at $y = z = 0$ as a function of x/h, panel (b) displays E_x^{tip} at $x = h$, $z = 0$ as a function of y/h, and panel (c) shows E_x^{tip} at $x = h$, $y = 0$ as a function of z/h (all calculated at $H = 10^4 h$ and $\varepsilon_x = \varepsilon_y = \varepsilon_z$).

V_{cr} increases about two times in the presence of water on the crystal surface, which is caused by its much higher permittivity. The fact that the critical voltage is lower for $LiTaO_3$ than for

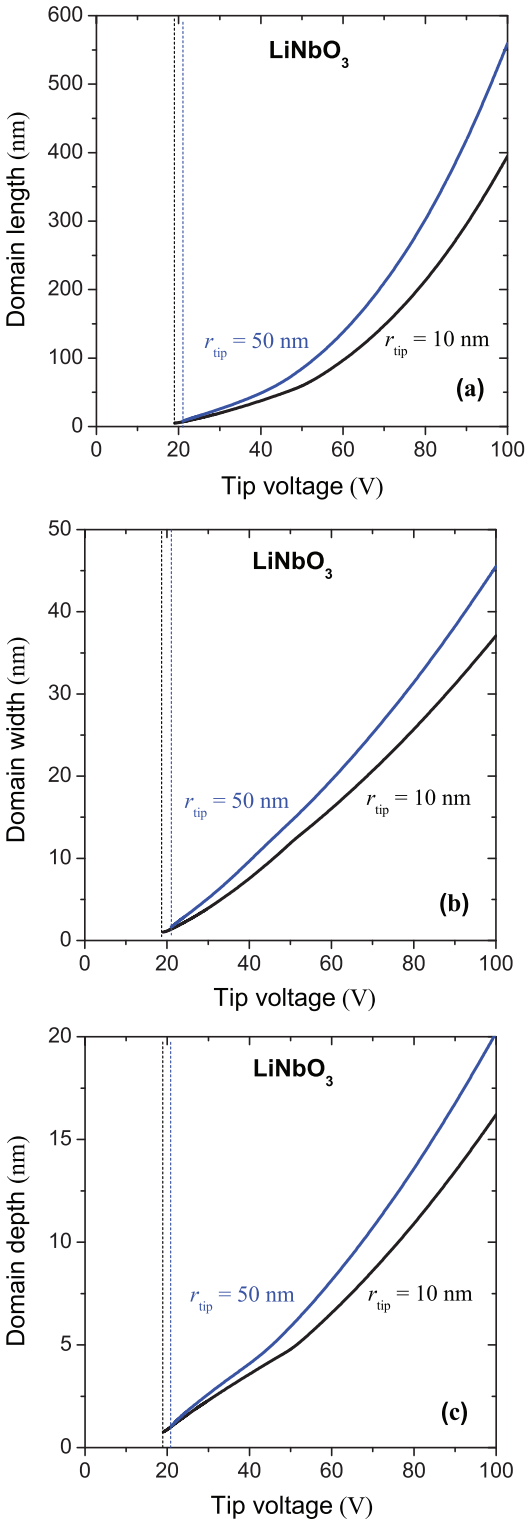

FIG. 3. (Color online) Equilibrium length (a), width (b), and depth (c) of a subsurface 180° domain in $LiNbO_3$ calculated as a function of voltage applied between the SFM tip and the bottom electrode. Conducting tips with radii of curvature indicated on the plot are assumed to be in direct contact with the crystal surface surrounded by air.

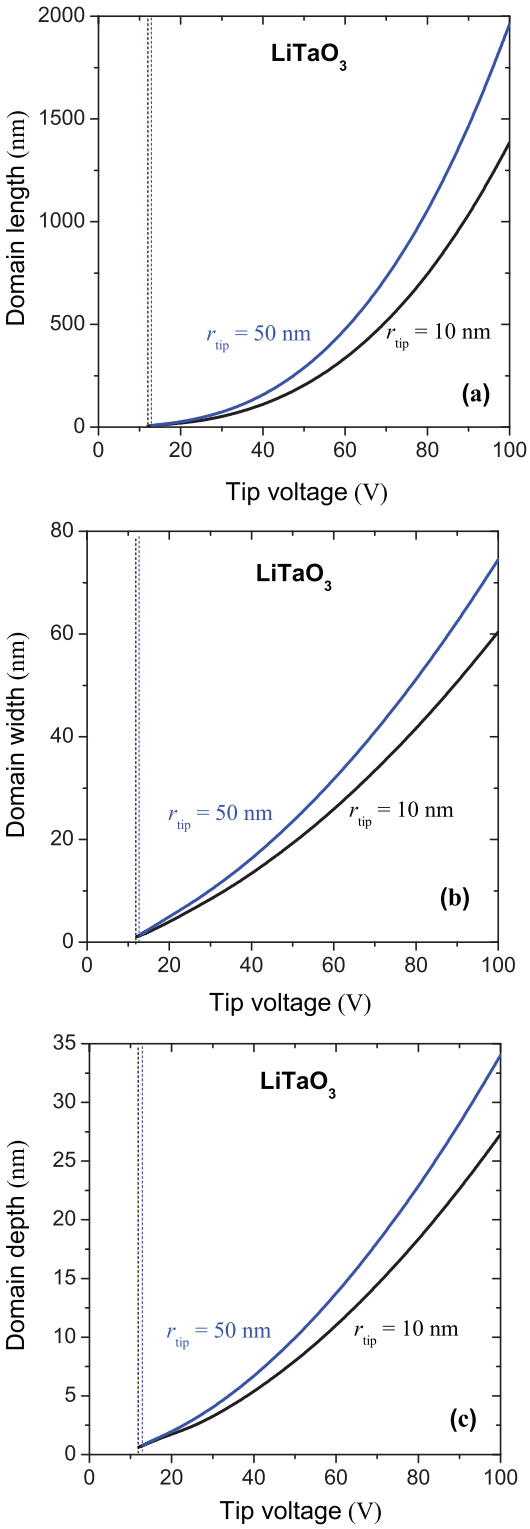

FIG. 4. (Color online) Equilibrium length (a), width (b), and depth (c) of a subsurface 180° domain in $LiTaO_3$ calculated as a function of tip voltage. Conducting tips with radii of curvature indicated on the plot are assumed to be in direct contact with the crystal surface surrounded by air.

$LiNbO_3$ can be attributed to a smaller value of the domain-wall energy γ in the former.

Figures 3 and 4 show the calculated equilibrium dimensions of subsurface domains in $LiNbO_3$ and $LiTaO_3$ as a function of tip voltage. The comparison of presented plots demonstrates

that the domain length L^* is always much larger than transverse domain sizes, exceeding the width w^* by $5-25$ times in the studied voltage range. At the same time, the width w^* is about two times bigger than the depth d^*, but the ratio w^*/d^* generally differs from 2 considerably. Hence, the subsurface domain cannot be accurately modeled by a half of an ellipsoid of revolution. As expected, all domain dimensions increase monotonically with increasing tip voltage. Although near the critical voltage the domain length $L^* \sim 10$ nm only, at $V = 100$ V it reaches values as high as about 550 nm in $LiNbO_3$ and 2000 nm in $LiTaO_3$ when $r_{tip} = 50$ nm. The equilibrium depth d^* does not exceed ~30 nm so that 180° domains written by the SFM tip appear to be "shallow" in bulk crystals. It should be noted that the theory also predicts that the presence of water on the crystal surface significantly increases equilibrium domain dimensions, especially the domain length that reaches about 2 μm in $LiNbO_3$ and 7 μm in $LiTaO_3$ at $V = 100$ V when $r_{tip} = 50$ nm.

In summary, we demonstrated theoretically that unusual 180° domains can be created in uniaxial ferroelectrics with the aid of a scanning force microscope. In contrast with conventional domains, where the polarization is orthogonal to the crystal surface,[6] these domains are polarized along the surface and situated asymmetrically with respect to the SFM tip. Although the written subsurface domains become energetically unfavorable after switching off the tip voltage, they cannot fully disappear owing to potential barriers hindering the motion of domain walls in the crystal lattice[2] and their pinning by defects. Moreover, domain stability can be enhanced by moving the biased SFM tip along the crystal surface in a direction parallel to the polar axis, which should result in the formation of a cylindrical 180° domain with a negligible depolarizing field. A system of such parallel domains may be useful for advanced device applications of $LiNbO_3$ and $LiTaO_3$ crystals. For example, periodically poled $LiNbO_3$ for the near-ultraviolet range may require antiparallel domains with a high aspect ratio and submicron sizes. These can be easily arranged by the described method using a moving SFM tip. High throughput can be achieved by using an array of identical cantilevers similar to those used in the "Millipede" approach.[26] To the best of the authors' knowledge, no systematic study of the formation and stability of the in-plane subsurface domains has been reported so far.

ACKNOWLEDGMENTS

The work at St. Petersburg State Polytechnical University was supported by the Federal Target Program "Research and development on priority directions of scientific-technological complex of Russia for 2007–2013." The work at Aveiro University was supported by the Portuguese Science and Technology Foundation (FCT) within the project PTDC/CTM-NAN/121313/2010. The activities in CICECO were partly supported by the FCT grant PEst-C/CTM/LA011/2013.

*Corresponding author. Email address: pertsev.domain@mail.ioffe.ru
†Also at Ural Federal University, Lenin Ave. 51, Ekaterinburg 620083, Russia.

[1] J. Padilla, W. Zhong, and D. Vanderbilt, Phys. Rev. B **53**, R5969 (1996).
[2] B. Meyer and D. Vanderbilt, Phys. Rev. B **65**, 104111 (2002).
[3] P. Paruch, T. Tybell, and J.-M. Triscone, Appl. Phys. Lett. **79**, 530 (2001).
[4] K. Tanaka, Y. Kurihashi, T. Uda, Y. Daimon, N. Odagawa, R. Hirose, Y. Hiranaga, and Y. Cho, Jpn. J. Appl. Phys. **47**, 3311 (2008).
[5] A. Gruverman and A. L. Kholkin, Rep. Prog. Phys. **69**, 2443 (2006).
[6] S. V. Kalinin, A. N. Morozovska, L. Q. Chen, and B. J. Rodriguez, Rep. Prog. Phys. **73**, 056502 (2010).
[7] C. Durkan, M. E. Welland, D. P. Chu, and P. Migliorato, Phys. Rev. B **60**, 16198 (1999).
[8] M. Molotskii, J. Appl. Phys. **93**, 6234 (2003).
[9] M. Molotskii, A. Agronin, P. Urenski, M. Shvebelman, G. Rosenman, and Y. Rosenwaks, Phys. Rev. Lett. **90**, 107601 (2003).
[10] A. Yu. Emelyanov, Phys. Rev. B **71**, 132102 (2005).
[11] A. N. Morozovska, E. A. Eliseev, and S. V. Kalinin, Appl. Phys. Lett. **89**, 192901 (2006).
[12] L. Arizmendi, Phys. Status Solidi A **201**, 253 (2004).
[13] V. Gopalan, M. J. Kawas, M. C. Gupta, T. E. Schlesinger, and D. D. Stancil, IEEE Photonics Technol. Lett. **8**, 1704 (1996).
[14] J. B. Thaxter, P. H. Carr, and J. H. Silva, IEEE Trans. Ultrason. Ferroelectr. Freq. Control **35**, 525 (1988).
[15] L. A. Bursill and P. J. Lin, Ferroelectrics **70**, 191 (1986).
[16] S. Belaidi, P. Girard, and G. Leveque, J. Appl. Phys. **81**, 1023 (1997).
[17] E. J. Mele, Am. J. Phys. **69**, 557 (2001).
[18] I. V. Lindell, K. I. Nikoskinen, and A. Viljanen, IEE Proc-A: Sci, Meas Technol **144**, 156 (1997).
[19] R. Landauer, J. Appl. Phys. **28**, 227 (1957).
[20] H. W. Hao, A. M. Baro, and J. J. Saenz, J. Vac. Sci. Technol. B **9**, 1323 (1991).
[21] N. A. Pertsev, A. Petraru, H. Kohlstedt, R. Waser, I. K. Bdikin, D. Kiselev, and A. L. Kholkin, Nanotechnology **19**, 375703 (2008).
[22] L. D. Landau, E. M. Lifshitz, and L. P. Pitaevskii, *Electrodynamics of Continuous Media* (Pergamon, Oxford, 1984).
[23] T. Otto, S. Grafström, and L. M. Eng, Ferroelectrics **303**, 149 (2004).
[24] D. A. Scrymgeour, V. Gopalan, A. Itagi, A. Saxena, and P. J. Swart, Phys. Rev. B **71**, 184110 (2005).
[25] D. Lee, H. Xu, V. Dierolf, V. Gopalan, and S. R. Phillpot, Phys. Rev. B **82**, 014104 (2010).
[26] P. Vettiger, G. Cross, M. Despont, U. Drechsler, U. Durig, B. Gotsmann, W. Haberle, M. A. Lantz, H. E. Rothuizen, R. Stutz, and G. K. Binnig, IEEE Trans. Nanotechnol. **1**, 39 (2002).